Impact of damping on the superconducting gap dynamics induced by intense terahertz pulses

Tianbai Cui, Xu Yang, Chirag Vaswani, Jigang Wang, Rafael M. Fernandes, and Peter P. Orth

Phys. Rev. B **100**, 054504 — Published 5 August 2019

DOI: 10.1103/PhysRevB.100.054504

Impact of damping on superconducting gap dynamics induced by intense terahertz pulses

Tianbai Cui,[1] Xu Yang,[2,3] Chirag Vaswani,[2,3] Jigang Wang,[2,3] Rafael M. Fernandes,[1] and Peter P. Orth[2,3]

[1] *School of Physics and Astronomy, University of Minnesota, Minneapolis, Minnesota 55455, USA*
[2] *Department of Physics and Astronomy, Iowa State University, Ames, Iowa 50011, USA*
[3] *Ames Laboratory, U.S. DOE, Iowa State University, Ames, Iowa 50011, USA*

We investigate the interplay between coherent gap dynamics and damping in superconductors taken out of equilibrium by strong optical pulses with sub-gap terahertz frequencies. A semi-phenomenological formalism is developed to include the damping within the electronic subsystem that arises from effects beyond Bardeen-Cooper-Schrieffer (BCS) mean-field theory, such as interactions between Bogoliubov quasi-particles and decay of the Higgs mode. These processes, conveniently expressed as longitudinal T_1 and transverse T_2 relaxation times in the standard pseudospin language for superconductors, cause the gap amplitude to be suppressed after the pulse is turned off, but before the time scale where thermalization occurs due to coupling to the lattice. We show that our model quantitatively captures the experimental gap dynamics reported here of NbN and Nb_3Sn through the picosecond time scale.

I. INTRODUCTION

The coherent control of non-equilibrium states of interacting quantum matter promises far-reaching capabilities by turning on (or off) desired electronic material properties. A particular focus in this field has been the manipulation of superconductivity by non-equilibrium probes. While earlier works showed that microwave pulses could be used to enhance the superconducting transition temperature T_c of thin superconducting films,[1–3] recent advances in ultrafast pump-and-probe techniques opened the possibility of investigating superconductivity in the pico- and femto-second timescales by coherent light pulses.[4–13] Such coherent pulses have been employed to manipulate the electronic and lattice properties of quantum materials, resulting in transient behaviors that are consistent with the onset of non-equilibrium superconductivity above T_c.[14–16] Alternatively, coherent pulses have also been employed to assess the coherent dynamics of the superconducting state.[7,9,17–26]

In Ref. 7, a single-cycle intense THz pulse resonant with the superconducting gap Δ was applied to a thin film of the conventional s-wave superconductor NbN, reporting coherent gap oscillations with frequency 2Δ. This was followed by a slow decrease of the gap, possibly associated with thermalization of the energy absorbed from components of the pump with frequencies larger than 2Δ. To maintain coherence and avoid excess heating, it is thus advantageous to apply longer, multi-cycle pulses with exclusively sub-gap frequency components,[8,9] where Cooper pairs cannot be broken into quasi-particle Bogoliubov excitations via single photon absorption processes. In the absence of pair-breaking and on sufficiently short timescales before thermalization effects with the environment set in, the electronic state is then expected to evolve in the manifold of Bardeen-Cooper-Schrieffer (BCS) states. This coherent time evolution can be conveniently recast in terms of Anderson pseudospins[27] precessing around a pseudo-magnetic field that is modified by the optical pulse.

Here, we report such an experimental study of superconducting gap dynamics in thin films of NbN and Nb_3Sn using intense, multi-cycle sub-gap THz pulses in a hitherto unexplored regime of large THz field amplitudes of up to 109 kV/cm. This allows for substantial light-control of the gap, even for initial temperatures far below the superconducting transition temperature T_c, where initial thermal quasi-particle excitations are absent. We focus our study on the regime of coherent gap dynamics, which occurs on timescales less than 20 picoseconds. This is complementary to an interesting earlier study by Beck *et al.* in Ref. 8 using ultra-narrow sub-gap terahertz pulses with GHz linewidths that focused on longer timescales of hundreds of picoseconds. That study reported an enhancement of the gap at intermediate temperatures due to a redistribution of thermally excited quasi-particles.

We complement our experimental work with detailed theoretical modeling that can phenomenologically capture all the salient features observed experimentally. This includes damping and decoherence effects that arise from residual, integrability-breaking interactions within the electronic system, which are not captured within the BCS approximation. In particular, our results shed light on the two different relaxation timescales that are inherent to the observed dynamics. We show that these are markedly shorter than lattice relaxation rates, but consistent with rapid relaxation that occurs within the electronic subsystem.

Specifically, we study superconducting gap dynamics in thin films of NbN and Nb_3Sn subjected to intense THz fields with sub-gap spectra. Our data reveals that while the pump is on, the gap oscillates at a frequency equal to twice the pump frequency. This previously observed behavior is well-described by the solution to the time-dependent BCS equation, which naturally gives rise to gap oscillations.[18–21,28–40] When the pump is turned off, however, the gap oscillations quickly disappear in the

experiment, yet the gap amplitude continues to be suppressed, while remaining finite. These behaviors, particularly the latter one, are at odds with the non-equilibrium BCS dynamics, which predicts the gap to display coherent oscillation with slow collisionless relaxation around a constant average value.[18,28,31,32,41] We want to emphasize that our experimental observations are consistent with previous studies[7] employing single-cycle pulses, but they are more pronounced at the large pump fluences that we employ.

To elucidate this behavior, we develop a semi-phenomenological model that captures not only the coherent evolution of the gap function in the picosecond time scale, but also damping and decoherence effects in the time scale of tens of picoseconds. Because this time scale precedes the thermalization with the lattice degrees of freedom, the relevant relaxation processes must arise solely within the electronic subsystem from effects not captured by BCS. These include interactions between Bogoliubov quasi-particles and the coupling between the Higgs (amplitude) mode and the continuum. In the pseudospin notation, we identify two types of relaxation process: the longitudinal relaxation T_1, corresponding to relaxation of quasi-particles, and the transverse relaxation T_2, corresponding to relaxation of the gap. While the main effect of T_2 is to suppress the gap oscillations after the pump is turned off, the main impact of T_1 in this regime is to decrease the average gap value. We show that the previously observed gap dynamics in NbN for single-cycle pulses, reported in Ref. 7, can also be quantitatively described within our semi-phenomenological model. To get similar quantitative agreement for multi-cycle pulse experiments in both NbN and Nb_3Sn, we need to introduce an additional phenomenological parameter η that describes the dissipation of heat out of the electronic subsystem into the environment. We find that for off-resonant multi-cycle pump pulses, where the amount of energy that is deposited by the pump is large, about 30% of the energy is rapidly dissipated to the environment.

The paper is organized as follows: we first summarize the experimental results in Sec. II. Then, we introduce our theoretical modeling and present a thorough analysis it in Sec. III. In Sec. IV, we perform a detailed theory-experiment comparison, before drawing our conclusions in Sec. V. Details about the experimental setup and pseudospin formalism are provided in Appendices A and B, respectively.

II. EXPERIMENTAL RESULTS

We probe the superconducting gap dynamics in NbN and Nb_3Sn using intense THz pump, weak THz probe ultrafast spectroscopy. Our NbN sample is a 120 nm thick NbN film grown on (100)-oriented MgO single crystalline substrates via pulsed laser deposition, as previously reported in Ref. 42. An interesting study of the non-linear optical response in NbN can also be found in Ref. 43.

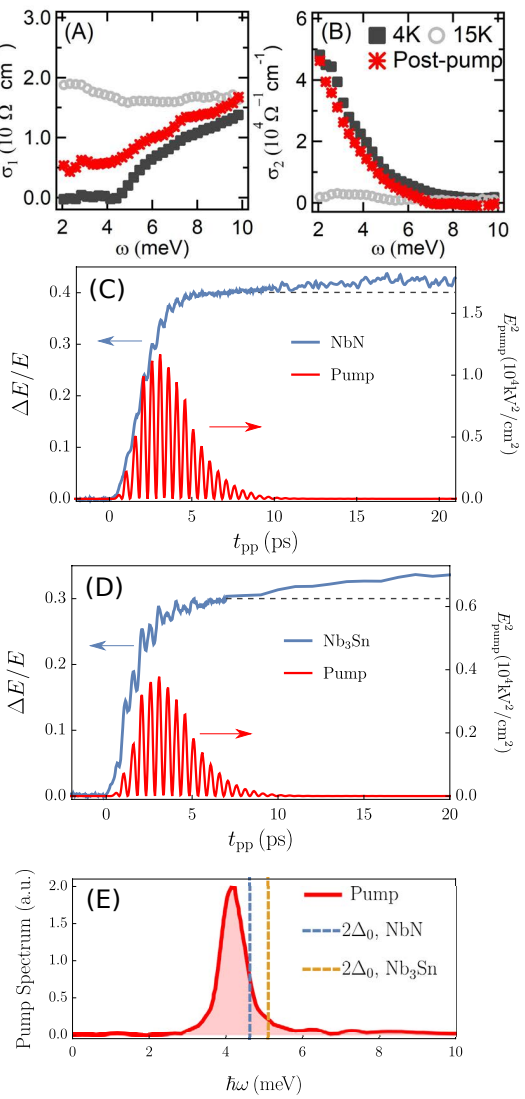

FIG. 1. (Color online) Experimental results of time-domain THz pump-probe spectroscopy on NbN and Nb_3Sn thin films. Panels (A) and (B) show the real and imaginary parts of the optical conductivity σ_1 and σ_2 in NbN. Gray curves are equilibrium results at $T = 4$ K $< T_c = 13$ K (dark gray), and $T = 15$ K $> T_c$ (light gray). The red curve is taken $t_{pp} = 10$ ps after a strong multi-cycle THz pump with peak electric field $E_{pump} = 109$ kV/cm and duration $\tau = 10$ ps (shown in panel (C)). (C) Relative pump-induced change of transmitted probe field strength $\Delta E/E$ (blue curve) in NbN at fixed t_{gate}. The red curve shows the pump profile. (D) $\Delta E/E$ versus t_{pp} at fixed t_{gate} in Nb_3Sn (blue curve). The red curve shows the pump profile, with a peak electric field of $E_{pump} = 62$ kV/cm. (E) Frequency spectrum of the multi-cycle pump pulses. Most of the spectral weight lies below the optical gap in both NbN and Nb_3Sn (vertical lines). The weight at Δ_0, corresponding to the frequency of the Higgs (amplitude) mode, is also small.

The Nb_3Sn sample is a thinner film that is only 20 nm thick and was grown by magnetron sputtering on a 1 mm

Al_2O_3 (100) substrate.[10] The superconducting transition temperatures in equilibrium are $T_c(\mathrm{NbN}) \approx 13$ K and $T_c(Nb_3Sn) \approx 16$ K, respectively. We extract the optical conductivity in equilibrium and non-equilibrium from the complex transmission using a scanning gate pulse delay t_{gate}. By varying the optical delay t_{pp} between the pump and the probe pulses, we track the ultrafast dynamics of the superconducting gap $\Delta(t)$ on picosecond timescales. Additional experimental details are given in Appendix A.

Let us first discuss the experimental results for NbN. The behavior of the real and imaginary parts of the optical conductivity, $\sigma_1(\omega)$ and $\sigma_2(\omega)$, of NbN is shown in Fig. 1 (A)-(B). In equilibrium (gray curves), the onset of superconductivity below $T_c(\mathrm{NbN}) \approx 13$ K is signaled by the opening of an optical gap in $\sigma_1(\omega)$ and by a $1/\omega$ dependence of $\sigma_2(\omega)$ at low frequencies. The gap reaches a low-temperature value of $2\Delta(\mathrm{NbN}) \approx 4.6$ meV at $T \ll T_c$.[42] We then expose the sample to an intense, multi-cycle THz pump shown in Fig. 1 (C), whose spectral weight lies mostly below the optical gap (see Fig. 1 (E)). The post-pump state (red curve in panels (A, B)) exhibits larger values of $\sigma_1(\omega)$ within the 2Δ range, and slightly reduced values of $\sigma_2(\omega)$, due to the quench of the SC condensate.

To extract the ultrafast dynamics of the gap function $\Delta(t_{pp})$, we prepare the system in equilibrium at $T = 4$ K, expose it to an intense multi-cycle THz pump pulse and measure the relative change of the transmitted electric field amplitude of a delayed THz probe pulse due to the presence of the pump

$$\Delta E(t_{pp})/E \equiv \big[E(\text{pump on}, t_{pp}) - E(\text{off})\big]/E(\text{off}) \quad (1)$$

at a fixed gate time t_{gate}. In equilibrium, the relative change of the probe field transmission $\Delta E(T)/E \equiv [E(T) - E(T_0)]/E(T_0)$ with fixed (variable) temperature T_0 (T) was shown to faithfully reflect the behavior of the superconducting gap $\Delta E(T)/E \propto [\Delta(T) - \Delta_0]/\Delta_0$,[6,9] where $\Delta_0 \equiv \Delta(T_0)$ and we use $T_0 = 4$ K. It was shown that this relationship also holds in non-equilibrium.[6] We determine the numerical value of the proportionality factor α in $\Delta E(t_{pp})/E = \alpha\big[1 - \Delta(t)/\Delta_0\big]$ by extracting the superconducting gap $\Delta(t)$ in non-equilibrium at $t_{pp} = 10$ ps from a fit of the optical conductivity in Figs. 1(A, B) to a generalized Mattis-Bardeen theory.[44] We find a numerical value of $\alpha_{\mathrm{NbN}} = 2.7$.

In Fig. 1(C), we show the observed ultrafast time evolution of $\Delta E/E = \alpha_{\mathrm{NbN}}[1 - |\Delta(t)|/\Delta_0]$ (blue curve), with initial state $\Delta_0 \equiv \Delta(T_0 = 4\ \mathrm{K}, t = 0)$ well inside the superconducting state. We also plot the applied pump pulse (red curve) in order to show that the gap $\Delta(t)$ oscillates with twice the pump frequency while the pump pulse is on. Interestingly, after the pump is turned off, the oscillations disappear quickly, and, most importantly, $\Delta(t)$ continues to decrease on the time scale of tens of picoseconds. This behavior continues before the gap eventually returns to its initial equilibrium value on nanosecond time scales *via* equilibration with phonons. This latter regime is not discussed in this paper.

Let us now describe our experimental results of Nb_3Sn, which are shown in Fig. 1(D). We expose the 20 nm thick Nb_3Sn films, that are initially prepared at low temperatures $T_0 = 4\ \mathrm{K} \ll T_c$ well inside the superconducting phase, to the same intense, multi-cycle THz pulse that we used for NbN. As the optical gap in Nb_3Sn is even larger $2\Delta(Nb_3Sn) = 5.1$ meV,[10] the spectral weight of the pump pulse lies almost fully inside the gap (see Fig. 1 (E)). As a result, pair-breaking (by single photons) can be safely neglected. As shown in Fig. 1(D), we observe the same salient features as for NbN, which were described above. The suppression of the gap oscillations and the decrease of the average gap after the pulse has passed, however, are now even more pronounced. We note that we determine α_{Nb_3Sn} from $\Delta E(T)/E$ and find $\alpha_{Nb_3Sn} = 0.75$.

We would like to emphasize that although the pump pulse we used has a temporal width of the order of the inverse gap, the non-equilibrium dynamics is still far from the adiabatic regime. This is due to the fact that, for multi-cycle pulses, the characteristic time scale of the perturbation is determined by the period of the cycle, and the width of the pulse is less relevant. This is in sharp contrast to single-cycle pulses, where the characteristic time scale is determined by the pulse width.[18] We will theoretically analyze this issue systematically in the next section.

We note that, although the $\Delta E/E$ curve in Fig. 1(C) remains above the dashed line after the pump is off, the data displays noticeable noise. Such a noise likely arises from the high intensity of the pump used. Note, however, that using similarly high-intensity pumps, the data on NbSn3 shown in Fig. 1(D) is much less noisy, and displays the same decrease of the gap after the pump is turned off. Importantly, a similar behavior was reported previously in Ref. 7 for less intense single-cycle THz pulse experiments on NbN films. Notably, after the single-cycle pulse has passed, the average gap was reported to continue to decrease, an observation that was already mentioned explicitly in Ref. 7. Thus, the suppression of the gap after the pump is turned off seems to be a much more generic occurrence in pump-and-probe experiments

III. THEORETICAL MODEL AND ANALYSIS

To model and understand the experimental results presented in Sec. II, we first resort to standard time-dependent BCS theory. As shown in detail below, this fully coherent approach, however, is unable to properly describe the experimental results. In particular, it cannot account for the rapid suppression of the gap oscillations and the continuing decrease of the average gap after the pump has passed. This motivates our new phenomenological approach that introduces two relaxation timescales T_1 and T_2 to include additional damping. This yields a much more accurate, quantitative description of the gap dynamics, for single-cycle pump pulses. To ob-

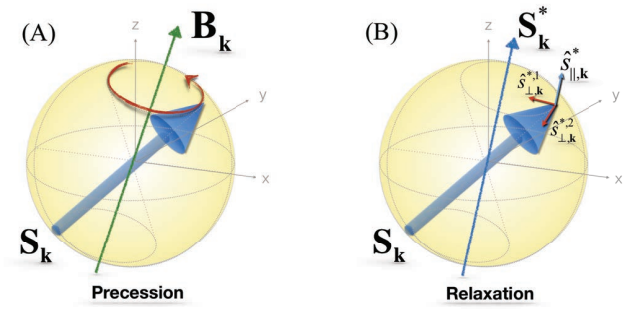

FIG. 2. (A) Schematics of fully coherent pseudospin precession under the time-dependent pseudo-magnetic field $\boldsymbol{B}_\boldsymbol{k}$ (green). (B) Schematics of the pseudospin relaxation towards the thermalized configuration $\boldsymbol{S}^*_\boldsymbol{k}$ showing the different effects of T_1 and T_2 processes.

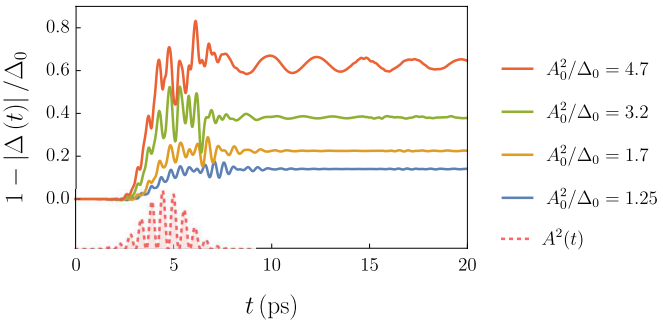

FIG. 3. (Color online) Undamped BCS gap dynamics induced by multi-cycle THz pulses of various amplitude A_0^2/Δ_0. The pump pulse has duration $\tau = 10\pi/\Delta_0 = 8$ ps, width $\sigma = \tau/6$, center frequency $\omega_p = 1.65\Delta_0$ with $\Delta_0 = 2.55$ meV $= 2\pi \times 0.62$ THz. Its profile is shown at the bottom (red dashed). During the pump, the gap exhibits oscillations with multiples of $2n\omega_p$. While at lower amplitudes the $n = 1$ component is dominant, higher order $n > 1$ components (mainly $n = 2$) are non-zero for larger amplitudes $A_0^2/\Delta_0 = 3.2, 4.7$. After the pump, the gap exhibits slowly (algebraically) damped oscillations with frequency $2\Delta_\infty$ and increasing amplitude for increasing pump amplitude A_0.

tain quantitative agreement between theory and experiment for (off-resonant) multi-cycle pulses, we introduce an additional parameter η describing dissipation of energy out of the electronic subsystem into the environment. The timescales $T_{1,2}$ we extract from our "fit" turn out to be of the order of the pulse width, consistent with relaxation processes that occur within the electronic subsystem.

A. Coherent dynamics from the BCS model

Let us now explain our theoretical modeling in more detail. The starting point of our theoretical analysis is the BCS Hamiltonian

$$H_{\rm BCS} = \sum_{\boldsymbol{k},\sigma} \xi_{\boldsymbol{k}+e\boldsymbol{A}} c^\dagger_{\boldsymbol{k},\sigma} c_{\boldsymbol{k},\sigma} + \sum_{\boldsymbol{k}} \left(\Delta c^\dagger_{\boldsymbol{k},\uparrow} c^\dagger_{-\boldsymbol{k},\downarrow} + \text{h.c.}\right) + \frac{|\Delta|^2}{V_0} \tag{2}$$

with square-lattice dispersion $\varepsilon_\boldsymbol{k} = -2J(\cos k_x + \cos k_y)$. Here, we have defined $\xi_\boldsymbol{k} = \varepsilon_\boldsymbol{k} - \mu$, and the chemical potential is set to $\mu = -1.18J$, corresponding to approximately quarter-filling. We note that the precise form of the energy dispersion is not important in the following, as we choose a filling sufficiently far away from the van Hove point and a generic light polarization. The superconducting order parameter obeys the self-consistency equation

$$\Delta = -V_0 \sum_{\boldsymbol{k}} \langle c_{-\boldsymbol{k},\downarrow} c_{\boldsymbol{k},\uparrow} \rangle \,, \tag{3}$$

where $V_0 > 0$ denotes an attractive interaction. In NbN and Nb_3Sn its origin is presumably rooted in electron-phonon interactions. For the calculations in this paper, we set $V_0 = 3J$ and the Debye frequency $\omega_{\rm D} = J/2$, yielding $\Delta_0 = 0.08J$ and $T_c = 0.048J$. The electronic density of states is almost constant in a window of size of the Debye frequency around the Fermi energy.

The pump laser field is included in the Hamiltonian via the vector potential $\boldsymbol{A}(t)$. In our experiment, it takes the form

$$\boldsymbol{A}(t) = \hat{\boldsymbol{e}}_{\rm p} A_0 \theta(t)\theta(\tau - t) \exp\left[-\frac{(t-\tau/2)^2}{2\sigma^2}\right] \cos(\omega_{\rm p} t) \tag{4}$$

with linear polarization vector $\hat{\boldsymbol{e}}_{\rm p}$, center frequency $\omega_{\rm p}$, temporal width σ, and duration τ. The values of these parameters in the various simulations we perform are given in the figure captions.

To describe the gap dynamics, we introduce Anderson pseudospins[27]

$$\boldsymbol{S}_\boldsymbol{k} = \psi^\dagger_\boldsymbol{k} \frac{\boldsymbol{\sigma}}{2} \psi_\boldsymbol{k} \tag{5}$$

with $\psi^\dagger_\boldsymbol{k} = (c^\dagger_{\boldsymbol{k},\uparrow}, c_{-\boldsymbol{k},\downarrow})$ being a Nambu spinor and $\boldsymbol{\sigma}$ a vector of Pauli matrices. The Hamiltonian (2) then reads

$$H_{\rm BCS} = -\sum_{\boldsymbol{k}} \boldsymbol{B}_\boldsymbol{k} \cdot \boldsymbol{S}_\boldsymbol{k} + \frac{|\Delta|^2}{V_0} + \sum_{\boldsymbol{k}} \bar{\xi}_{\boldsymbol{k},\boldsymbol{A}} \tag{6}$$

with pseudo-magnetic field

$$\boldsymbol{B}_\boldsymbol{k} = -2(\Delta', -\Delta'', \bar{\xi}_{\boldsymbol{k},\boldsymbol{A}}) \tag{7}$$

where $\Delta = \Delta' + i\Delta''$, and $\bar{\xi}_{\boldsymbol{k},\boldsymbol{A}} = \frac{1}{2}(\varepsilon_{\boldsymbol{k}+e\boldsymbol{A}} + \varepsilon_{\boldsymbol{k}-e\boldsymbol{A}}) - \mu$. Note that the pseudo-magnetic field depends on the state of the pseudospins via the gap equation: $\Delta = -V_0 \sum_\boldsymbol{k} \langle S^-_\boldsymbol{k} \rangle$ (see Eq. (3)).

In the initial equilibrium state, all pseudospins are aligned with the field direction $\boldsymbol{B}_\boldsymbol{k}$. Explicit expressions of the equilibrium spin state, and further details on the calculation are provided in Appendix B. The pump pulse $\boldsymbol{A}(t)$ then drives the system out of equilibrium by changing the band dispersion term via $B^z_\boldsymbol{k}$. Considering the time evolution governed by the standard BCS

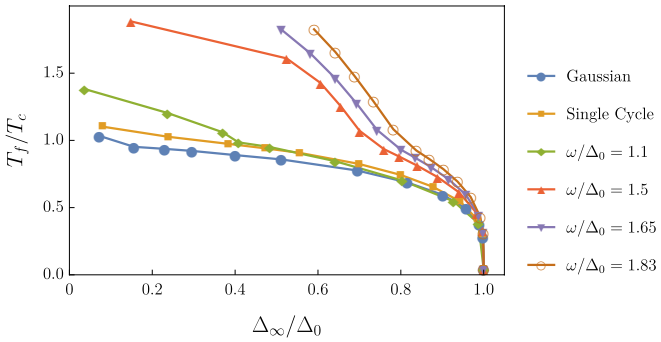

FIG. 4. (Color online) Final equilibrium temperature T_f (normalized to T_c) as a function of gap quench amplitude Δ_∞/Δ_0 for undamped BCS model ($T_1 = T_2 = \infty$). Temperature T_f is obtained from the energy deposited by the pulse [see Eq. (11)], and different Δ_∞ are obtained by changing A_0. The different pulse types are parametrized by $(\tau, \sigma, \omega_p) = (2\pi/\Delta_0, \tau/8, 0)$ for the Gaussian pulse, $(10\pi/\Delta_0, \tau/5, 1.3\Delta_0)$ for the single-cycle pulse, and $(10\pi/\Delta_0, \tau/6, \omega_p)$ with ω_p given in the figure for the multi-cycle pulses. The polarization of the electric field is along $\hat{x}$.

Hamiltonian (6) only, the pseudospins coherently precess around the new field direction $\boldsymbol{B_k}(t)$ according to the Bloch equation (see also[18,28,30,32,33,35–38]):

$$\frac{d\langle \boldsymbol{S_k}\rangle}{dt} = \langle \boldsymbol{S_k}\rangle \times \boldsymbol{B_k}\,. \tag{8}$$

We schematically depict the resulting coherent pseudospin dynamics in Fig. 2(A). Importantly, the pseudospin dynamics is immediately fed back into the pseudomagnetic field via the gap equation (3). Due to parity symmetry, only even-order terms of $\boldsymbol{A}(t)$ appear,[27,45] and the oscillation frequency of the gap during the pump is a multiple of $2\omega_\mathrm{p}$. This can be clearly seen in Fig. 3, which shows a numerical solution of $\Delta(t)$ for different amplitudes A_0. The dynamical behavior while the pulse is turned on is in agreement with our experimental results in Fig. 1, except for the highest amplitudes.

While the gap oscillations with frequency $2\omega_\mathrm{p}$ in the presence of the pump are correctly captured, there are crucial, qualitative differences between the BCS-theoretical and the experimental gap dynamics in Fig. 1. One difference is that while the BCS-theoretical gap displays coherent, slowly decaying oscillations with an amplitude that is increasing with increasing A_0, experimentally the gap oscillations are absent once the pump is off in our multi-cycle experiments.

The most important *qualitative* difference, however, is that the average BCS-theoretical gap is completely flat after the pump pulse has passed, while the gap amplitude continues to decrease in the experiment. The long-time average (theoretical) gap is often denoted Δ_∞, and its value depends on the fluence A_0 of the pulse. The discrepancy between the theory and the data occurs for both NbN and Nb_3Sn thin films, which have different thicknesses, driven by either multi- or single-cycle pump pulses,[7] and for different values of the pump intensity (for instance, the pump intensity is one order of magnitude smaller in the case of single-cycle pulses). Given that the Nb_3Sn sample is far cleaner than the NbN films (elastic low-temperature scattering rates are $\Gamma_{\mathrm{dis,\ Nb_3Sn}} \approx 7$ meV[10] and $\Gamma_{\mathrm{dis,\ NbN}} \approx 70$ meV), it is rather unlikely that the origin of the described phenomena lies in disorder-induced spatial gap inhomogeneities in the post-pump state. In addition, we do not observe the characteristic overshoot of the real part of the optical conductivity σ_1 in the post-pump state over the normal

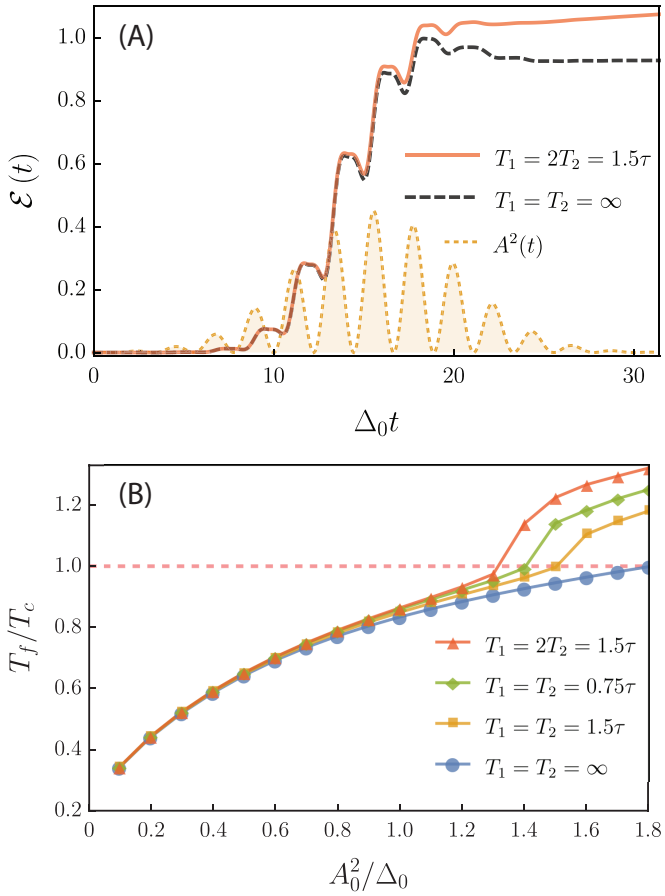

FIG. 5. (Color online) (A) Time evolution of the internal energy $\mathcal{E}$ of the electronic system arising from the energy deposited by a multi-cycle pump pulse $A^2(t)$ (orange dashed) with amplitude $A_0^2/\Delta_0 = 1.1$, duration $\tau = 10\pi/\Delta_0$, width $\sigma = \tau/5$, and center frequency $\omega_p = 1.41\Delta_0$. The polarization of the electric field is along $\hat{x}$ and we set $\eta = 1$. Different curves correspond to $T_1 = T_2 = \infty$ (black dashed) and $T_1 = 2T_2 = 1.5\tau$ (orange solid) as indicated. The energy is normalized by $N_f\Delta_0^2$, where N_f is the density of states at the Fermi level. (B) The effective temperature after the pump is turned off, $T_f \equiv T^*(\tau)$, normalized by T_c, as a function of the pump intensity A_0^2 for various T_1 and T_2. For finite $T_{1,2}$, the system will relax to the normal state once $T_f > T_c$, which leads to an increased energy absorption, as indicated by the change of slope of T_f when crossing the red dashed line. The pulse parameters are identical to the ones in panel (A).

state, that is associated with spatial inhomogeneities and can be reproduced using Brüggemann's effective medium theory.[17]

The diversity of experimental setups showing the same effect suggests that it may have a common origin. One possible culprit is pair-breaking promoted by the pump, which is not included in the formalism above and would naturally lead to a suppression of the gap. While one cannot completely rule out this mechanism, particularly in the single-cycle case, where the pump frequency is comparable to 2Δ, our Fig. 1(E) shows that in the multi-cycle experiments nearly all the spectral weight of the pump is below 2Δ. As a result, we search for a different mechanism that does not require pair-breaking.

B. Phenomenological account of damping in pseudo-spin dynamics

To account for the experimental observations, we thus go beyond the standard BCS description and include phenomenologically damping in the pseudospin equations of motion. The microscopic origin of these terms will be discussed below. In analogy with the general problem of spin precession, we introduce longitudinal (T_1) and transverse (T_2) relaxation rates:

$$\frac{d\langle \boldsymbol{S_k}\rangle}{dt} = \langle \boldsymbol{S_k}\rangle \times \boldsymbol{B_k} - \frac{\langle \boldsymbol{S_k}\rangle \cdot \hat{\boldsymbol{s}}^*_{\parallel,\boldsymbol{k}} - |\langle \boldsymbol{S^*_k}\rangle|}{T_1}\hat{\boldsymbol{s}}^*_{\parallel,\boldsymbol{k}} - \sum_{i=1}^{2}\frac{\langle \boldsymbol{S_k}\rangle \cdot \hat{\boldsymbol{s}}^{*,i}_{\perp,\boldsymbol{k}}}{T_2}\hat{\boldsymbol{s}}^{*,i}_{\perp,\boldsymbol{k}}\,. \tag{9}$$

Here,

$$\langle \boldsymbol{S^*_k}\rangle\big[T^*(t)\big] = \frac{1}{2}\hat{\boldsymbol{s}}^*_{\parallel,\boldsymbol{k}}\big[T^*(t)\big]\tanh\Big(\frac{\sqrt{\xi^2_{\boldsymbol{k}}+\Delta^2_*}}{2T^*(t)}\Big) \tag{10}$$

is the thermalized pseudospin configuration at time t at an effective temperature T^* with gap value $\Delta_* \equiv \Delta(T^*)$. The two vectors $\hat{\boldsymbol{s}}^{*,i}_{\perp,\boldsymbol{k}}$ with $i = 1,2$ span the plane perpendicular to the equilibrium pseudospin direction $\hat{\boldsymbol{s}}^*_{\parallel,\boldsymbol{k}}\big[T^*(t)\big]$. This is schematically depicted in Fig. 2(B) (see also Appendix B). Physically, the time scale T_1 is related to a redistribution of the quasi-particles, whereas the time scale T_2 is related to the dephasing of the off-diagonal quasi-particle coherence, which governs the damping of the gap oscillations. We note that the notion of quasi-particles depends on the choice of Bogoliubov transformation that one performs as the gap evolves in time. Here, we refer to the transformation that diagonalizes the Hamiltonian for the thermalized gap value $\Delta(T^*)$ at effective temperature T^*.

To compute $\hat{\boldsymbol{s}}^*_{\parallel,\boldsymbol{k}}$ and the effective temperature T^*, we first consider that all the energy deposited in the electronic subsystem by the pump is converted into a change in the internal energy (see also Ref. 41):

$$\mathcal{E}(t) = \langle H_{\rm BCS}(t)\rangle_{A=0} - \langle H_{\rm BCS}\rangle_{\rm init}\,. \tag{11}$$

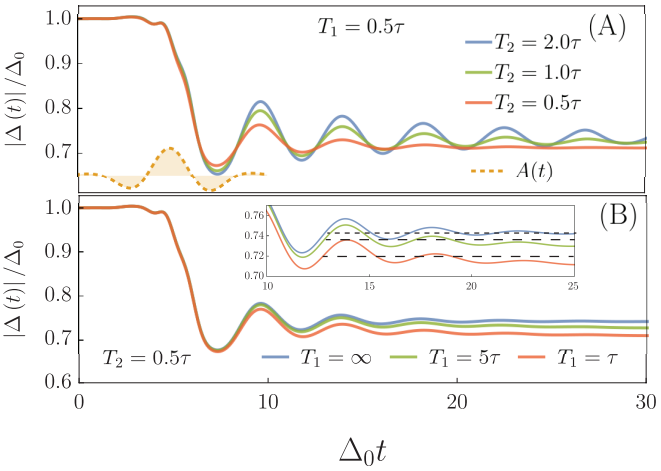

FIG. 6. (Color online) Theoretical results for the gap dynamics $\Delta(t)/\Delta_0$ for short single-cycle Gaussian pump pulses with duration $\tau = 10/\Delta_0$ and width $\sigma = \tau/5$. Here, Δ_0 denotes the initial equilibrium gap value at $t = 0$. In panel (A), we keep $T_1 = 0.5\tau$ fixed and change T_2, whereas in panel (B) we set $T_2 = 0.5\tau$ and vary T_1. The pump pulse shape $A(t)$ is shown at the bottom of panel (A) (dashed). We set the pump amplitude to be $A_0 = \sqrt{1.12\Delta_0}$ in both panels. Inset in panel (B) highlights the post-pump behavior of the gap. One clearly observes deviations of the average gap value from the horizontal black dashed lines for finite T_1.

Here, the expectation value is calculated in the time-evolved BCS state according to Eq. (9) and $\langle H_{\rm BCS}\rangle_{\rm init}$ is the initial ground state energy. From $\mathcal{E}(t)$, we extract both $T^*(t)$ and $\Delta_*(t) \equiv \Delta[T^*(t)]$, which are themselves function of time while the pump is turned on. Specifically, we use that the energy of the BCS state at temperature T is given by

$$\mathcal{E}(T) = \sum_{\boldsymbol{k}}\Big[\xi_{\boldsymbol{k}} - \big(1-2n_F[E_{\boldsymbol{k}}(T)]\big)E_{\boldsymbol{k}}(T)\Big] + \frac{|\Delta(T)|^2}{V_0}\,, \tag{12}$$

where $n_F(E) = 1/(\exp(E/T)+1)$ is the Fermi function, $E_{\boldsymbol{k}}(T) = \sqrt{\xi^2_{\boldsymbol{k}} + |\Delta(T)|^2}$ is the quasi-particle energy and the equilibrium gap $\Delta(T)$ is determined from the finite temperature gap equation $1 = V_0\sum_{\boldsymbol{k}}\frac{\tanh(E_{\boldsymbol{k}}/2T)}{2E_{\boldsymbol{k}}}$. We then obtain Δ_* and T^* by setting $\mathcal{E}(t) = \mathcal{E}(T^*) - \mathcal{E}(T=0)$ and solving for these variables.[31] Here we used that $\langle H_{\rm BCS}\rangle_{\rm init} \equiv \mathcal{E}(T=0)$ in our simulation. Once the pump is turned off, energy is no longer deposited in the electronic subsystem, and thus $T^*(t>\tau) = T^*(\tau) \equiv T_f$, and $\Delta_*(t>\tau) \equiv \Delta_f$.

We have calculated T_f for a variety of Gaussian pulse shapes parametrized by τ, σ, ω_p and amplitudes A_0. In Fig. 4, we present the resulting T_f/T_c as a function of the long-time (average) non-equilibrium value of the gap Δ_∞/Δ_0 for different pulse shapes. Clearly, the amount of energy that is deposited into the system for a given quench amplitude of the gap $(1-\Delta_\infty/\Delta_0)$ strongly depends on the pulse shape. Less energy is deposited if the

pulse is resonant with the Higgs (amplitude) mode, which occurs if it contains frequency components $\omega_p \approx \Delta_0$. The different behaviors can thus be grouped into two classes corresponding to resonant and off-resonant driving. Resonant pulses are short Gaussian pulses and single-cycle pulses with $\Delta_0\sigma \lesssim 1$, where σ is the width of the pulse, and longer multi-cycle pulses with center frequency $\omega_p \approx \Delta_0$. On the other hand, if the center frequency of the multi-cycle pulse is not resonant with the Higgs (amplitude) mode, the deposited energy is much larger. In order to quantitatively describe experimental data for off-resonant multi-cycle pulses, we will therefore introduce a third phenomenological parameter $0 < \eta \leq 1$, where $1-\eta$ describes the fraction of energy that is dissipated from the electronic system into the environment. Thus, η describes the fraction of the energy that remains within the electronic subsystem. On short timescales, this energy loss can occur via scattering with electronic quasi-particles that are located outside the volume excited by the pump pulse. We found this time scale to be consistent with T_1.

Interestingly, the presence of relaxation also affects the amount of energy that is deposited into the electronic system during a pulse. In Fig. 5(A), we show the electronic energy $\mathcal{E}(t)$ for a multi-cycle pulse with center frequency $\omega_p = 1.4\Delta_0$ with and without relaxation, *i.e.*, for finite and infinite T_1 and T_2. We observe that more energy is deposited for finite $T_{1,2}$. This occurs as the faster damping of the Higgs (amplitude) mode generates excess quasiparticles that directly couple with light, which leads to greater energy absorption. In Fig. 5(B), we show how the final temperature T_f depends on the pump fluence A_0^2. As expected, for sufficiently strong pump pulses, the superconducting state can be completely melted by heating and $T_f > T_c$. Once this threshold is reached, the slope of the curves $T_f(A_0)$ becomes steeper, corresponding to a more rapid increase of T_f with increasing fluence in the normal state.

To elucidate how T_1 and T_2 affect the gap dynamics, and disentangle the contributions from these two relaxation processes, we systematically explore their effects in Fig. 6. For concreteness and to make connection to earlier experiments using single-cycle pulses,[7] we consider a resonant single-cycle Gaussian-shaped pulse of duration $\tau = 10/\Delta_0 \approx 3$ ps, width $\sigma = \tau/5$ and center frequency $\omega_p = 1.3\Delta_0$. In Fig. 6(A), we fix $T_1 = 0.5\tau$ and vary T_2. It is apparent that the main effect of T_2 is to suppress the post-pump gap oscillations, while the decay of the average gap value after the pump is off is largely unaffected by changing T_2. Conversely, in Fig. 6(B), we keep $T_2 = 0.5\tau$ constant and vary T_1. While for $T_1 = \infty$ the average gap value is essentially constant after the pump is off, when $T_1 \sim \tau$ the average gap shows a clear and continuous suppression at long times. This behavior is highlighted in the inset. Note also that the amplitude of the post-pump gap oscillations are little affected by changing T_1.

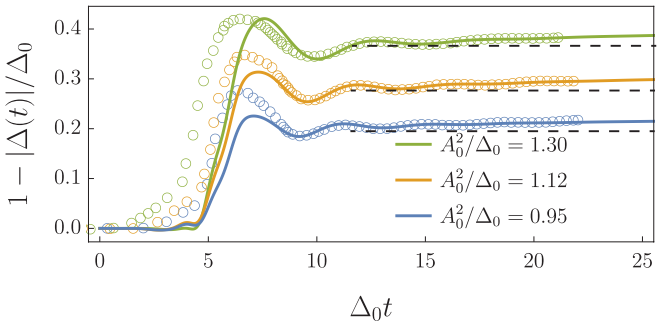

FIG. 7. (Color online) Comparison between theory (solid lines) and single-cycle pump experiments on NbN published in Ref. 7 (data points are for fluences 5.6, 6.4, and 7.2 nJ/cm^2). We set $\tau = 10/\Delta_0$, $\sigma = \tau/5$ for the two lowest pump fluences and $\sigma = \tau/7$ for the highest one. We find good agreement using the phenomenological parameters $T_1 = 1.5\tau$ and $T_2 = 0.3\tau$. The horizontal and vertical experimental axes were rescaled as explained in the main text. Note that the average gap value decreases after the pulse is off, which is clearly seen by the deviation from the dashed horizontal lines.

IV. APPLICATION TO EXPERIMENTAL RESULTS

We now apply our semi-phenomenological approach to describe experimental results for both single and multi-cycle experiments, and extract the damping timescales T_1 and T_2 from experiment. The values of T_1 and T_2 describe characteristic timescales of integrability-breaking interactions within the electronic subsystem. Using the equations of motion (9), we are able to quantitatively describe the experimentally observed gap dynamics in NbN for resonant single-cycle pulses. In order to reach a quantitative description for experiments on NbN and Nb_3Sn using slightly off-resonant multi-cycle pulses, we introduce an additional phenomenological parameter η, describing rapid energy dissipation out of the electronic subsystem into the environment on picosecond timescales. Technically, we use $\eta\mathcal{E}(t)$ to calculate Δ^* and T^* and let the system relax towards the corresponding pseudospin configuration according to Eq. (10).

A. Comparison to resonant single-cycle pulse experiments

In Fig. 7, we demonstrate that our theory can quantitatively describe experimental results on NbN for short single-cycle pulses that were published in Ref. 7. Both the rapid damping of the oscillations and the continuing decrease of the average gap after the pump is off (shown by the increasing deviation from the dashed gray lines in the figure) can be quantitatively described by $T_1 = 1.5\tau$ and $T_2 = 0.3\tau$. These timescales are thus of the order of the pump duration which is approximately $\tau \approx 3$ ps. We do not need the additional parameter η, which is set to $\eta = 1$ here.

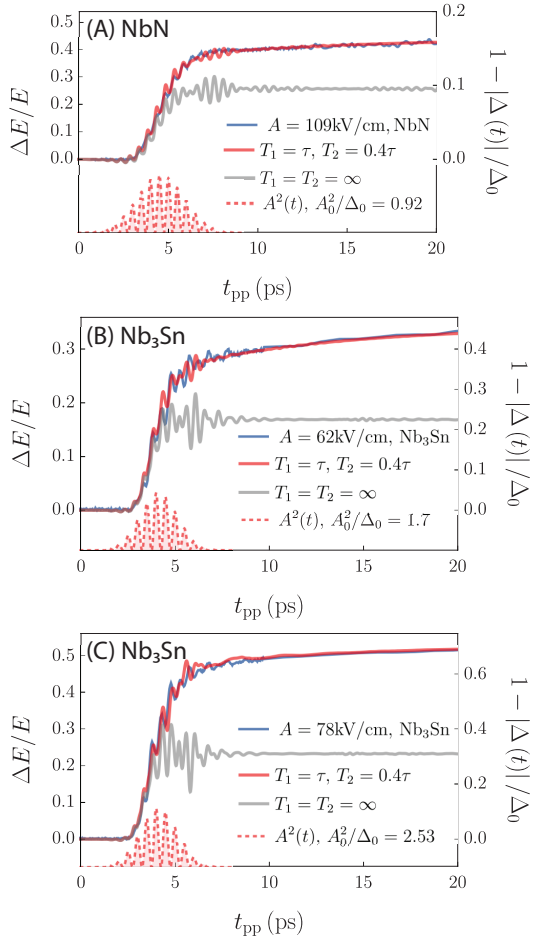

FIG. 8. (Color online) Theory-experiment comparison for slightly off-resonant multi-cycle pulses. Panel (A) is for NbN and panels (B, C) are for Nb_3Sn. The experimental trace of $\Delta E(t)/E$ is shown in blue and converted into $1 - |\Delta(t)|/\Delta_0 = \alpha^{-1}\Delta E/E$ using the procedure described in Sec. II with $\alpha_{\rm NbN} = 2.7$ and $\alpha_{\rm Nb_3Sn} = 0.75$. The gray line is obtained using pure BCS theory without any relaxation terms, and the red line is our phenomenological theory parametrized by relaxation parameters T_1, T_2 and η. In order to make quantitative comparison, the experimental traces are shifted to the right by 2.73 ps for NbN and 2.7 ps for Nb_3Sn to compensate the differences between the experimentally determined and the theoretically determined $t_{\rm pp}$. The duration and width of the Gaussian pump pulses (shown at the bottom) are $\tau = 10\pi/\Delta_0$ and $\sigma = \tau/5$ ($\tau/6$) for NbN (Nb_3Sn), and the center frequencies are $\omega_p = 1.83\Delta_0$ ($1.65\Delta_0$) for NbN (Nb_3Sn), which are taken from experiment. The polarization used in the theoretical calculation is along $\hat{x}$. We used an energy dissipation factor $\eta = 0.66, 0.72, 0.6$ for panels A, B, C. The other parameters $T_{1,2}$ and pump amplitude A_0^2 are given in the figure. We notice that the thermalized gap value $\Delta(T_f)$ is much smaller than the non-thermal BCS steady-state value Δ_∞, even though we use $\eta < 1$.[31]

To make this comparison, we have rescaled the time axis using the equilibrium gap value $\Delta_0 = 0.36$ THz in the experiment. The experimental y axis in Ref. 7, $\Delta E_{\rm probe} \propto 1 - \Delta(t)/\Delta_0$, is given in arbitrary units, and we have rescaled it by a factor of 0.345 (0.341) for the two lowest (the highest) pump fluence. We note that these rescaling factors yield the correct Δ_∞ within error bars, which were independently measured in the experiment. We note that Ref. 7 includes results for ΔE, while we report $\Delta E/E$ in our experiments to measure the gap. There is thus a proportionality factor between the two procedures, and we do not expect to find the same numerical value for $\alpha_{\rm NbN}$ in the two cases. Finally, we have shifted the origin of the experimental time t_{pp} axis by 1.73 ps, 1.68 ps and 1.36 ps for the three pump fluences 5.6, 6.4 and 7.2 nJ/cm^2, respectively, with respect to our simulations. This reflects the fact that t_{pp} is measured from the peak of the approximately 3 ps broad pump pulse, which occurs about halfway through the pulse.[7]

B. Comparison to slightly off-resonant multi-cycle pulse experiments

A direct comparison of our theory to experimental results for the gap dynamics induced by multi-cycle THz pump pulses in NbN and Nb_3Sn is shown in Figs. 8 and 9. The pulse parameters are set to their experimental values. Specifically, pulse durations and widths are $\tau = 10\pi/\Delta_0$ and $\sigma = \tau/5$ ($\tau/6$) and the center frequencies are $\omega_p = 1.83\Delta_0$ ($1.65\Delta_0$) for NbN (Nb_3Sn). The pump pulses are therefore slightly off-resonant with the Higgs (amplitude) mode, which occurs at $\omega = \Delta_0$. Here, $\Delta_0 = 2.3$ meV $= 2\pi \times 0.55$ THz for NbN, and $\Delta_0 = 2.55$ meV$=2\pi \times 0.62$ THz for Nb_3Sn. This results in a pump duration of $\tau = 9$ ps (8 ps) for NbN (Nb_3Sn). The pump profiles are shown in the figures. The pump pulse spectra are shown in Fig. 1(E), demonstrating that both pulses only carry small spectral weight at Δ_0 and above the optical gap $2\Delta_0$. As shown in Fig. 4, the amount of energy that is deposited in such an off-resonant multi-cycle pulse within BCS theory increases rapidly with an increasing gap quench amplitude $1 - \Delta_\infty/\Delta_0$. It exceeds the condensation energy (such that $T_f > T_c$) for $1 - \Delta_\infty/\Delta_0 \gtrsim 0.75$. In our theoretical analysis, we initially prepare the system in the equilibrium state at the initial experimental temperature $T = 4$ K, which is much smaller than T_c of both NbN and Nb_3Sn samples. The redistribution of initially present thermal quasi-particles due to the pump pulse, which was shown to be an important factor at intermediate temperatures,[8] is fully taken into account, but plays a minor role in our case as $T \ll T_c$.

We can fit the gap dynamics for multi-cycle pulses within our phenomenological model in two ways: (i) we introduce an additional parameter $\eta < 1$, which describes the fraction of the internal energy that remains in the electronic subsystem pumped by the laser. In this case, we find that the data can be well described using relaxation timescales T_1 and T_2 that are of the order of the pulse duration τ. This is just like in the fit to the resonant single-cycle pulses in Fig. 7, for which $\eta = 1$.

Alternatively, we (ii) enforce energy conservation within the electronic subsystem and set $\eta = 1$. To describe the data, we have to then use values of T_1 and T_2 that are about one order of magnitude larger than in the case of the resonant pulse.

In Fig. 8, we show theory-experiment comparison including the parameter $\eta < 1$. Besides the Nb_3Sn data shown in Fig. 1 (C), we also include data taken at a higher pump fluence. We find excellent quantitative agreement over the complete time interval and for all pump strengths. In contrast to the case with no damping, $T_1 = T_2 = \infty$ (gray lines), we find that the oscillations of $|\Delta(t)|$ are quickly suppressed after the pulse is turned off, and, more importantly, that a continuous and slow increase of $1 - |\Delta(t)|/\Delta_0$ takes place over the time scale of tens of picoseconds. The numerical values we obtain from comparing to the data are $\eta \approx 0.6 - 0.7$, and damping parameters that are of the order of the pulse width: $T_1 = \tau \approx 2T_2$, where $\tau \approx 10$ ps. The amplitude of the pulse is adjusted such that the final value of the gap matches the experimental one. Since the timescales $T_1, T_2 \lesssim \tau$, thermalization sets in while the pulse is on, and the undamped BCS result converges to a much smaller gap value at long times than the solution in the presence of relaxation.

In Fig. 9, we enforce energy conservation within the electronic subsystem by setting $\eta = 1$. Agreement is then limited to the time after the pump pulse is off and for not too large fluences. During the pulse and for large fluence, our phenomenological theory with $\eta = 1$ predicts gap oscillations with an amplitude that is larger than is observed experimentally. As $T_1, T_2 \gg \tau$, there is only a small difference between the damped and undamped gap dynamics while the pump is on. After the pulse, the damped solution slowly approaches the thermalized gap with a slope dictated by T_1, while the undamped solution is completely flat.

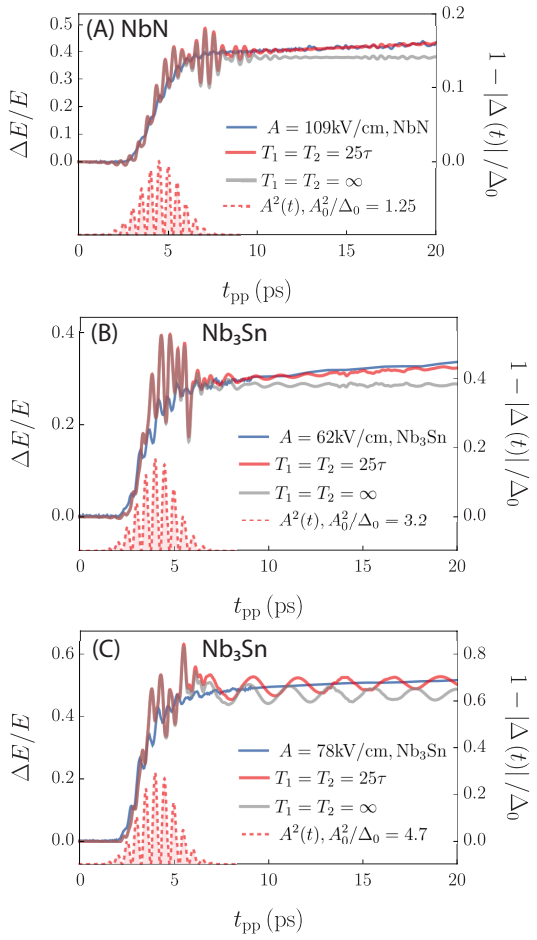

FIG. 9. (Color online) Theory-experiment comparison for slightly off-resonant multi-cycle pulses, enforcing energy conservation in the electronic subsystem by setting $\eta = 1$. Panel (A) is for NbN and panels (B, C) are for Nb_3Sn. Blue line corresponds to experimental data (see Fig. 8 for details), red line is the fit to the phenomenological theory with values for T_1 and T_2 given in the panels and $\eta = 1$. Gray line is the undamped BCS result. In order to make quantitative comparison, the experimental traces are shifted to the right by 2.41 ps for NbN and 2.1 ps for Nb_3Sn to compensate the differences between the experimentally determined and the theoretically determined t_{pp}. The values for the center frequency ω_p, pulse width σ and duration τ are equal to the ones in the corresponding panels of Fig. 8. For $\eta = 1$, the relaxation parameters T_1 and T_2 have to be chosen much larger than in Fig. 8, and the pump amplitude A_0 has to be also adjusted to a larger value. Good agreement between theory and experiment is limited to times after the pump pulse is off and to lower gap quench amplitudes (panels A and B). During the pulse and for larger quench amplitudes, the theory with $\eta = 1$ predicts gap oscillations that are too large compared to our experimental observations. The fact that T_1 and T_2 have to be set to much larger values than in Figs. 7 and 8 signals the need to include the dissipation parameter η in our theory to quantitatively describe gap dynamics for off-resonant multi-cycle pulses.

C. Summary of theory-experiment comparison

To summarize, using our phenomenological extension of BCS theory, we can quantitatively describe gap dynamics in resonant single-cycle experiments, both during and after the pump pulse (up to ≈ 20 ps, when additional relaxation mechanisms with the lattice set in). The extracted relaxation timescales T_1 and T_2 are found to have comparable values, which are of the order of the pulse duration $\tau = 10/\Delta_0 = 3$ ps. This is consistent with our assumption that the relaxation processes responsible for the behaviors observed experimentally take place within the electronic subsystem and are associated with the energy deposited in this subsystem while the pump is on. Our theory accounts both for the absence of gap oscillations after the pump pulse, and the overall decay of the average gap after the pump pulse has passed.

To describe off-resonant multi-cycle pulse experiments, we have performed two different fitting procedures: (i) by introducing an additional energy dissipation parameter

$\eta < 1$, we can quantitatively describe the experimental gap dynamics using $T_1 \approx 2T_2 \approx \tau$ that are again of the order of the pulse duration $\tau \approx 8$ ps. The dissipation parameter takes values of $\eta \approx 0.6-0.7$ corresponding to the fact that about 30% of the energy deposited by the pump pulse is dissipated to the environment on a timescales of τ. Alternatively, (ii) we have enforced energy conservation within the electronic subsystem by setting $\eta = 1$. In this case, we find that $T_1 = T_2 = 25\tau$ need to be chosen about an order of magnitude larger than before, and we find a reasonable but less quantitative description of the data. This suggests that rapid energy dissipation out of the electronic subsystem occurs in the experiment when off-resonant pumps are used, which must be taken into account theoretically.

Although T_1, T_2 and η are phenomenological quantities, it is important to discuss their possible microscopic origins. The key point is that the $T_{1,2}$ processes arise within the electronic subsystem, before equilibration with the lattice sets in. Because the BCS Hamiltonian is integrable,[32,46–49] any thermalization must arise from non-BCS effects. Residual interactions between the Bogoliubov quasi-particles, which are neglected in the mean-field BCS approach, could provide a mechanism for quasi-particle relaxation, which affects T_1. Moreover, the Higgs (amplitude) mode excited resonantly by the laser pump disperses into the quasi-particle continuum.[50,51] As a result, one expects damping of the amplitude mode, which should affect the T_2 process. The parameter η describes rapid dissipation of energy out of the electronic subsystem. One possible origin of this process is electronic scattering with electronic degrees of freedom that are outside of the pump excitation volume. The lateral focal size of the pump is 1.2 mm. Future work should address a more microscopic derivation of damping effects in non-equilibrium superconductors.

Our theory accounts both for the absence of gap oscillations after the pump pulse, and the overall decay of the average gap after the pump pulse has passed. As shown in Figs. 8 and 9, although the behavior after the pump is off is very well captured quantitatively by our model, there are discrepancies between the theoretical and experimental curves while the pump is on. They are more pronounced for stronger pump intensities. Whether they originate from interference effects between the external drive (with centering frequency ω_0) and the tendency of the (closed) system to oscillate with frequency Δ_∞, or are caused by a different non-linear effect, deserves further attention. Here, our focus is on the behavior after the pump pulse has passed.

V. CONCLUSIONS

In this paper, we established a semi-phenomenological framework that allows one to incorporate damping beyond BCS theory in the picosecond time-evolution of the gap function of an s-wave superconductor subject to an intense THz pulse. In the pseudospin language, damping arises from a longitudinal process T_1, which is related to quasi-particle relaxation, and from a transverse process T_2, which is related to dephasing of off-diagonal quasi-particle coherence. We have found that T_1 mainly affects the post-pump average gap value, while T_2 mainly affects the post-pump gap oscillations. In addition, to account for rapid dissipation of energy, which is deposited by the pump, out of the electronic subsystem, we introduce a third parameter η. We find that dissipation processes become important for off-resonant multi-cycle pulses, where the pump necessarily deposits a significant amount of energy in order to quench the gap.

We apply our theory to resonant single-cycle pump pulse experiments on NbN thin films, and to off-resonant multi-cycle pulse experiments on NbN and Nb_3Sn films. We find excellent quantitative agreement for T_1 and T_2 values that are comparable to the duration of the pump pulse, $\tau = 3(8)$ ps for single-cycle (multi-cycle) experiments. For off-resonant pump pulses, where the energy deposited exceeds the condensation energy, we find that about 30% of the energy is rapidly dissipated out of the electronic subsystem. Possible microscopic origins of these phenomenologically introduced processes are scattering of quasi-particles, interaction of the Higgs (amplitude) mode with the quasi-particle continuum, and interactions between quasi-particles inside and outside the focal region of the pump pulse. Future work should develop a microscopic underpinning of this phenomenological framework.

While the picosecond evolution of the gap function in NbN and Nb_3Sn is different than that expected for coherent BCS-like dynamics, we show that it is consistent with relaxation processes that arise within the electronic subsystem and have a time scale much shorter than lattice relaxation rates. Future application of this approach to different superconductors will shed light on the relevance of the distinct types of relaxation and dissipation processes for each system.

ACKNOWLEDGMENTS

We thank M. Schütt for fruitful discussions and N. P. Armitage for providing the sample. T.C. and R.M.F. are supported by the Office of Basic Energy Sciences, U.S. Department of Energy, under award DE-SC0012336. J.W. and X.Y. acknowledge supported by the Army Research office under award W911NF-15-1-0135 (THz spectroscopy). P.P.O. acknowledges support from Iowa State University Startup Funds. T.C. and R.M.F. acknowledge the Minnesota Supercomputing Institute (MSI) at the University of Minnesota, where the numerical calculations were performed.

Appendix A: Experimental details

The schematic experimental setup is shown in Fig. 10. The Ti-sapphire laser with 3 mJ pulse energy, 40 fs pulse duration, 1KHz repetition rate and 800 nm center wavelength is split into three optical paths for the purposes of pumping, probing and sampling, respectively. The terahertz (THz) pump pulse has a larger intensity, which is generated by tilted-pulse-front phase matching through 1.3% MgO doped $LiNbO_3$ crystal. In contrast, the THz probe pulse, generated by optical rectification through 1 mm thick (110)-ZnTe crystal, has a smaller intensity. The pump and probe pulses are at orthogonal polarizations. They focus on the sample at normal incidence and the focal sizes are 1.2 mm and 0.8 mm for the pump and the probe beam, respectively. After the sample, the transmitted pump beam is blocked by a wire grid polarizer while the transmitted probe E-field is measured by the electro-optic sampling. The transmitted E-field signal is integrated by a Boxcar integrator and sent to the DAQ board together with the on-off signal from two synchronized choppers. Further details can be found in Ref. 10, where the same experimental setup and data analysis method were used. Comparing with previous THz-pump-probe experiment on NbN thin film (e.g. Ref. 9), the peak E-field of narrow band 1THz pump can reach values as high as 109 kV/cm.

The ultrafast dynamics of the superconducting gap $\Delta(t_{pp})$ is tracked by fixing $t_{\rm gate}$ at the peak of the pump-induced change of the transmitted probe electric field,

$$\Delta E(t_{pp}) = E(\text{pump on}, t_{pp}, 4\text{ K}) - E(\text{off}, 4\text{ K})\,, \quad \text{(A1)}$$

and scanning the delay time $t_{\rm pp}$ between pump and probe. Here, $E(\text{pump on}, t_{pp}, 4\text{ K})$ corresponds to the transmitted probe electric field amplitude at fixed $t_{\rm gate}$ and variable t_{pp} for a system that was initially prepared at $T = 4$ K before it was exposed to the pump pulse. We note that our choice of $t_{\rm gate}$ corresponds to setting $t_{\rm gate}$ to the position of maximal contrast of the transmitted probe field signal with and without pump. As demonstrated in Refs. 6, 9, 10, and 17, the pump-probe signal $\Delta E/E$, where $E \equiv E(\text{off}, 4\text{ K})$, faithfully reflects the transient behavior of superconducting order parameter Δ. In other words, it holds that

$$\frac{\Delta E(t_{pp})}{E(\text{off}, T = 4\text{ K})} = \alpha\Big(1 - \frac{\Delta(t_{pp})}{\Delta(T = 4\text{K})}\Big) \quad \text{(A2)}$$

with approximately temperature-independent proportionality factor α.

We obtain the proportionality constant $\alpha_{\rm NbN} = 2.7$ for NbN as follows. We independently determine the gap Δ at $t_{pp} = 10$ ps from the optical conductivity $\sigma(t_{pp})$ shown in Fig. 1(a, b). We extract the gap $\Delta(t_{pp} = 10\text{ ps}) = 3.9/2 = 1.95$ meV from a fit of $\sigma_2(t_{pp})$ using the expressions in Ref.[44] derived for a BCS model with general scattering time τ in equilibrium. We first find the scattering rate $\tau^{-1}_{\rm NbN} = 72.8$ meV from fitting the equilibrium conductivity $\sigma(T = 15\text{ K})$ in the normal state to the same model. Comparing the value of $\Delta E/E = 0.41$ and $\Delta(t_{pp})/\Delta(4\text{K}) = 3.9/4.6 = 0.85$, we find $\alpha_{\rm NbN} = 2.7$.

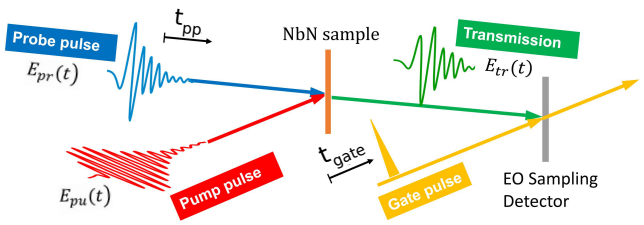

FIG. 10. Schematic of THz-pump-THz-probe measurement. $E_{\rm pu}(t)$, $E_{\rm pr}(t)$ and $E_{\rm tr}(t)$ are the time domain E-fields of the pump beam, the probe beam and the transmitted probe beam, respectively. $t_{\rm gate}$ is the relative time delay between the probe and the gate pulse. $t_{\rm pp}$ is the delay time between the pump and the probe.

For Nb_3Sn, we find the proportionality constant $\alpha_{\rm Nb_3Sn} = -0.75$ by first relating the change of the probe field transmission to the change of the gap in equilibrium:[6,9,17]

$$\frac{E(T) - E(T_0)}{E(T_0)} = \alpha\Big(1 - \frac{\Delta(T)}{\Delta(T_0)}\Big) \quad \text{(A3)}$$

with $T_0 = 4$ K. We find $E(4\text{K}) = -0.13$ and $E(18\text{K}) = -0.03$, which together with $\Delta(4\text{K}) = 5.1$ meV and $\Delta(18\text{K}) = 0$, yields $\alpha_{\rm Nb_3Sn} = -0.75$. We assume that the same relation also holds in non-equilibrium, as was shown explicitly for optical pulses.[6]

Appendix B: Pseudospin formalism and non-equilibrium dynamics

We start from the BCS Hamiltonian for superconductivity, which is written as Eq. (1) in the main text:

$$H_{\rm BCS} = \sum_{\boldsymbol{k},\sigma} \xi_{\boldsymbol{k}+e\boldsymbol{A}} c^\dagger_{\boldsymbol{k},\sigma} c_{\boldsymbol{k},\sigma} + \sum_{\boldsymbol{k}} \big(\Delta c^\dagger_{\boldsymbol{k},\uparrow} c^\dagger_{-\boldsymbol{k},\downarrow} + \text{h.c.}\big) + \frac{|\Delta|^2}{V_0} \quad \text{(B1)}$$

where $\xi_{\boldsymbol{k}} = \varepsilon_{\boldsymbol{k}} - \mu$ is the electronic dispersion near the Fermi level, e is the charge of the electron, which couples to an external electromagnetic field $\boldsymbol{A}$, and $V_0 > 0$ denotes the attractive superconducting interaction. The superconducting gap, Δ, is determined self-consistently via the gap equation:

$$\Delta = -V_0 \sum_{\boldsymbol{k}} \langle c_{-\boldsymbol{k},\downarrow} c_{\boldsymbol{k},\uparrow} \rangle \quad \text{(B2)}$$

In general, $\Delta = \Delta' + i\Delta''$ is a complex number, with Δ' and Δ'' being the real and imaginary part of the gap respectively. The phase is purely a gauge choice. Therefore, in equilibrium, the superconducting gap is usually chosen to be real for convenience.

In the presence of parity symmetry (i.e. $\xi_{\boldsymbol{k}} = \xi_{-\boldsymbol{k}}$ and $n_{\boldsymbol{k}} = n_{-\boldsymbol{k}}$), and using the pseudospin representation introduced by Anderson[27]

$$\begin{aligned} S^-_{\boldsymbol{k}} &= c_{-\boldsymbol{k},\downarrow} c_{\boldsymbol{k},\uparrow} \\ S^+_{\boldsymbol{k}} &= c^\dagger_{\boldsymbol{k},\uparrow} c^\dagger_{-\boldsymbol{k},\downarrow} \\ S^z_{\boldsymbol{k}} &= n_{\boldsymbol{k}} - \frac{1}{2} \end{aligned} \tag{B3}$$

with $n_{\boldsymbol{k}} = c^\dagger_{\boldsymbol{k},\uparrow} c_{\boldsymbol{k},\uparrow} + c^\dagger_{\boldsymbol{k},\downarrow} c_{\boldsymbol{k},\downarrow}$, the BCS Hamiltonian can be written as

$$H_{\mathrm{BCS}} = -\sum_{\boldsymbol{k}} \boldsymbol{B}_{\boldsymbol{k}} \cdot \boldsymbol{S}_{\boldsymbol{k}} + \frac{|\Delta|^2}{V_0} + \sum_{\boldsymbol{k}} \bar{\xi}_{\boldsymbol{k},\boldsymbol{A}} \,. \tag{B4}$$

The gap is self-consistently determined by a collective pseudospin coordinate

$$\Delta = -V_0 \sum_{\boldsymbol{k}} \langle S^-_{\boldsymbol{k}} \rangle \tag{B5}$$

The pseudo-magnetic field is given by $\boldsymbol{B}_{\boldsymbol{k}} = (-2\Delta', 2\Delta'', -\xi_{\boldsymbol{k}+e\boldsymbol{A}} - \xi_{\boldsymbol{k}-e\boldsymbol{A}})$. In equilibrium ($\boldsymbol{A} = 0$), the pseudospins perfectly align with the pseudo-magnetic field. Consequently, the expectation values of the pseudospins have the following configuration at $T = 0$:

$$\langle \boldsymbol{S}_{\boldsymbol{k}} \rangle_{T=0} = \tfrac{1}{2} \tfrac{\boldsymbol{B}_{\boldsymbol{k}}}{|\boldsymbol{B}_{\boldsymbol{k}}|} \tag{B6}$$

We assume this to be the initial state before the THz pump pulse. In equilibrium at finite temperature T, the length of the pseudospins is reduced, but they still point along the pseudo-magnetic field

$$\begin{aligned} \langle S^x_{\boldsymbol{k}} \rangle_T &= \frac{-\Delta'}{2E_{\boldsymbol{k}}} \tanh\left(\frac{E_{\boldsymbol{k}}}{2T}\right) \\ \langle S^y_{\boldsymbol{k}} \rangle_T &= \frac{\Delta''}{2E_{\boldsymbol{k}}} \tanh\left(\frac{E_{\boldsymbol{k}}}{2T}\right) \\ \langle S^z_{\boldsymbol{k}} \rangle_T &= -\frac{\xi_{\boldsymbol{k}}}{2E_{\boldsymbol{k}}} \tanh\left(\frac{E_{\boldsymbol{k}}}{2T}\right) \end{aligned} \tag{B7}$$

where $E_{\boldsymbol{k}}(T) = \sqrt{\xi^2_{\boldsymbol{k}} + |\Delta(T)|^2}$ is the quasi-particle dispersion, and the finite temperature gap $\Delta(T) = \Delta' + i\Delta''$ is determined by the gap equation

$$1 = V_0 \sum_{\boldsymbol{k}} \frac{\tanh[E_{\boldsymbol{k}}/(2T)]}{2E_{\boldsymbol{k}}} \,. \tag{B8}$$

The pseudospin formalism of the BCS model is particularly convenient for the study of non-equilibrium dynamics of the superconducting gap, since the pseudospin dynamics is described by the precession under the pseudo magnetic field:

$$\frac{d}{dt} \boldsymbol{S}_{\boldsymbol{k}} = i \left[H_{\mathrm{BCS}}, \boldsymbol{S}_{\boldsymbol{k}} \right] = \boldsymbol{S}_{\boldsymbol{k}} \times \boldsymbol{B}_{\boldsymbol{k}} \tag{B9}$$

The complexity, however, is encoded in the self-consistency condition of the pseudo-magnetic field. Since the superconducting gap depends on the pseudospin configuration in $\boldsymbol{k}$-space, the pseudo-magnetic field will also change over time.

The quench dynamics of the superconducting gap has been thoroughly studied under the BCS framework using a topological classification of the spectral polynomial.[31,32,48] Recently, such classification has also been applied to the gap dynamics in THz-pump-probe experiments.[41]

Once the system is driven out of equilibrium, the internal energy of the electronic system increases. One can calculate the superconducting gap $\Delta_* = |\Delta_*| e^{i\phi}$ at the effective temperature T_* corresponding to the internal energy at a given time, which uniquely determines the thermalized pseudospin configuration $\langle \boldsymbol{S}^*_{\boldsymbol{k}} \rangle = \frac{1}{2} \hat{\boldsymbol{s}}^*_{\parallel,\boldsymbol{k}} \tanh\left(\frac{\sqrt{\xi^2_{\boldsymbol{k}} + |\Delta_*|^2}}{2T^*(t)}\right)$, where

$$\hat{\boldsymbol{s}}^*_{\parallel,\boldsymbol{k}} = \left(\frac{-|\Delta_*| \cos\phi}{\sqrt{\xi^2_{\boldsymbol{k}} + |\Delta_*|^2}}, \frac{|\Delta_*| \sin\phi}{\sqrt{\xi^2_{\boldsymbol{k}} + |\Delta_*|^2}}, \frac{-\xi_{\boldsymbol{k}}}{\sqrt{\xi^2_{\boldsymbol{k}} + |\Delta_*|^2}} \right) , \tag{B10}$$

where $\Delta = \Delta' + i\Delta'' = |\Delta| e^{i\phi}$. Note that since the internal energy is changing over time, $\langle \boldsymbol{S}^*_{\boldsymbol{k}} \rangle$ and $\hat{\boldsymbol{s}}^*_{\parallel,\boldsymbol{k}}$ are also time dependent and generally not aligned with the pseudo-magnetic field $\boldsymbol{B}_{\boldsymbol{k}}$. Without damping, the pseudospin will simply precess around the self-consistent pseudo-magnetic field, which itself is also oscillating. Once damping is incorporated, the pseudo-spins tend to relax towards the thermalized configuration $\langle \boldsymbol{S}^*_{\boldsymbol{k}} \rangle$, which is described by Eq. (9) in the main text.

[1] G. M. Eliashberg, Sov. Phys. JETP **11**, 696 (1960).
[2] J. A. Pals, K. Weiss, P. M. T. M. van Attekum, R. E. Horstman, and J. Wolter, Phys. Rep. **89**, 323 (1982).
[3] B. I. Ivlev, S. G. Lisitsyn, and G. M. Eliashberg, J. Low Temp. Phys. **10**, 449 (1973).
[4] C. Giannetti, M. Capone, D. Fausti, M. Fabrizio, F. Parmigiani, and D. Mihailovic, Adv. Phys. **65**, 58 (2016).
[5] T. Kampfrath, K. Tanaka, and K. A. Nelson, Nat. Photon. **7**, 680 (2013).
[6] M. Beck, M. Klammer, S. Lang, P. Leiderer, V. V. Kabanov, G. N. Gol'tsman, and J. Demsar, Phys. Rev. Lett. **107**, 177007 (2011).
[7] R. Matsunaga, Y. I. Hamada, K. Makise, Y. Uzawa, H. Terai, Z. Wang, and R. Shimano, Phys. Rev. Lett. **111**, 057002 (2013).
[8] M. Beck, I. Rousseau, M. Klammer, P. Leiderer, M. Mittendorff, S. Winnerl, M. Helm, G. N. Gol'tsman, and J. Demsar, Phys. Rev. Lett. **110**, 267003 (2013).

[9] R. Matsunaga, N. Tsuji, H. Fujita, A. Sugioka, K. Makise, Y. Uzawa, H. Terai, Z. Wang, H. Aoki, and R. Shimano, Science **345**, 1145 (2014).

[10] X. Yang, C. Vaswani, C. Sundahl, M. Mootz, P. Gagel, L. Luo, J. H. Kang, P. P. Orth, I. E. Perakis, C. B. Eom, and J. Wang, Nat. Mater. **17**, 586 (2018).

[11] X. Yang, X. Zhao, C. Vaswani, C. Sundahl, B. Song, Y. Yao, D. Cheng, Z. Liu, P. P. Orth, M. Mootz, J. H. Kang, I. E. Perakis, C.-Z. Wang, K.-M. Ho, C. B. Eom, and J. Wang, Phys. Rev. B **99**, 094504 (2019).

[12] F. Giorgianni, T. Cea, C. Vicario, C. P. Hauri, W. K. Withanage, X. Xi, and L. Benfatto, Nat. Phys. (2019).

[13] M. Šindler, C. Kadlec, P. Kužel, K. Ilin, M. Siegel, and H. Němec, Phys. Rev. B **97**, 054507 (2018).

[14] R. Mankowsky, A. Subedi, M. Forst, S. O. Mariager, M. Chollet, H. T. Lemke, J. S. Robinson, J. M. Glownia, M. P. Minitti, A. Frano, M. Fechner, N. A. Spaldin, T. Loew, B. Keimer, A. Georges, and A. Cavalleri, Nature **516**, 71 (2014).

[15] W. Hu, S. Kaiser, D. Nicoletti, C. R. Hunt, I. Gierz, M. C. Hoffmann, M. Le Tacon, T. Loew, B. Keimer, and A. Cavalleri, Nat. Mater. **13**, 705 (2014).

[16] M. Mitrano, A. Cantaluppi, D. Nicoletti, S. Kaiser, A. Perucchi, S. Lupi, P. Di Pietro, D. Pontiroli, M. Riccò, S. R. Clark, D. Jaksch, and A. Cavalleri, Nature **530**, 461 EP (2016).

[17] R. Matsunaga and R. Shimano, Phys. Rev. Lett. **109**, 187002 (2012).

[18] T. Papenkort, V. M. Axt, and T. Kuhn, Phys. Rev. B **76**, 224522 (2007).

[19] T. Papenkort, T. Kuhn, and V. M. Axt, J. Phys. **193**, 012050 (2009).

[20] M. Zachmann, M. D. Croitoru, A. Vagov, V. M. Axt, T. Papenkort, and T. Kuhn, New J. Phys. **15**, 055016 (2013).

[21] A. Akbari, A. P. Schnyder, D. Manske, and I. Eremin, Europhys. Lett. **101**, 17002 (2013).

[22] M. Dzero, M. Khodas, and A. Levchenko, Phys. Rev. B **91**, 214505 (2015).

[23] Y. Murakami, P. Werner, N. Tsuji, and H. Aoki, Phys. Rev. B **93**, 094509 (2016).

[24] V. Gurarie, Phys. Rev. Lett. **103**, 075301 (2009).

[25] H. Krull, N. Bittner, G. S. Uhrig, D. Manske, and A. P. Schnyder, Nat. Comm. **7**, 11921 (2016).

[26] K. Katsumi, N. Tsuji, Y. I. Hamada, R. Matsunaga, J. Schneeloch, R. D. Zhong, G. D. Gu, H. Aoki, Y. Gallais, and R. Shimano, Phys. Rev. Lett. **120**, 117001 (2018).

[27] P. W. Anderson, Phys. Rev. **112**, 1900 (1958).

[28] A. F. Volkov and S. M. Kogan, J. Exp. Theor. Phys. **38**, 1018 (1974).

[29] M. H. S. Amin, E. V. Bezuglyi, A. S. Kijko, and A. N. Omelyanchouk, Low Temp. Phys. **30**, 661 (2004).

[30] R. A. Barankov, L. S. Levitov, and B. Z. Spivak, Phys. Rev. Lett. **93**, 160401 (2004).

[31] R. A. Barankov and L. S. Levitov, Phys. Rev. Lett. **96**, 230403 (2006).

[32] E. A. Yuzbashyan, B. L. Altshuler, V. B. Kuznetsov, and V. Z. Enolskii, J. Phys. A: Math. Gen. **38**, 7831 (2005).

[33] G. L. Warner and A. J. Leggett, Phys. Rev. B **71**, 134514 (2005).

[34] A. V. Andreev, V. Gurarie, and L. Radzihovsky, Phys. Rev. Lett. **93**, 130402 (2004).

[35] E. A. Yuzbashyan, B. L. Altshuler, V. B. Kuznetsov, and V. Z. Enolskii, Phys. Rev. B **72**, 220503(R) (2005).

[36] A. F. Kemper, M. A. Sentef, B. Moritz, J. K. Freericks, and T. P. Devereaux, Phys. Rev. B **92**, 224517 (2015).

[37] H. Krull, D. Manske, G. S. Uhrig, and A. P. Schnyder, Phys. Rev. B **90**, 014515 (2014).

[38] B. Fauseweh, L. Schwarz, N. Tsuji, N. Cheng, N. Bittner, H. Krull, M. Berciu, G. S. Uhrig, A. P. Schnyder, S. Kaiser, and D. Manske, ArXiv e-prints (2017), arXiv:1712.07989.

[39] M. A. Müller, P. Shen, M. Dzero, and I. Eremin, Phys. Rev. B **98**, 024522 (2018).

[40] J. A. Scaramazza, P. Smacchia, and E. A. Yuzbashyan, Phys. Rev. B **99**, 054520 (2019).

[41] Y.-Z. Chou, Y. Liao, and M. S. Foster, Phys. Rev. B **95**, 104507 (2017).

[42] B. Cheng, L. Wu, N. J. Laurita, H. Singh, M. Chand, P. Raychaudhuri, and N. P. Armitage, Phys. Rev. B **93**, 180511 (2016).

[43] C. Zhang, B. Jin, J. Han, I. Kawayama, H. Murakami, X. Jia, L. Liang, L. Kang, J. Chen, P. Wu, and M. Tonouchi, New Journal of Physics **15**, 055017 (2013).

[44] U. S. Pracht, E. Heintze, C. Clauss, D. Hafner, R. Bek, D. Werner, S. Gelhorn, M. Scheffler, M. Dressel, D. Sherman, B. Gorshunov, K. S. Il'in, D. Henrich, and M. Siegel, IEEE Transactions on Terahertz Science and Technology **3**, 269 (2013).

[45] J. Bardeen, L. N. Cooper, and J. R. Schrieffer, Phys. Rev. **108**, 1175 (1957).

[46] E. A. Yuzbashyan, V. B. Kuznetsov, and B. L. Altshuler, Phys. Rev. B **72**, 144524 (2005).

[47] E. A. Yuzbashyan, O. Tsyplyatyev, and B. L. Altshuler, Phys. Rev. Lett. **96**, 097005 (2006).

[48] E. A. Yuzbashyan and M. Dzero, Phys. Rev. Lett. **96**, 230404 (2006).

[49] N. A. Sinitsyn, E. A. Yuzbashyan, V. Y. Chernyak, A. Patra, and C. Sun, Phys. Rev. Lett. **120**, 190402 (2018).

[50] T. Cea, C. Castellani, G. Seibold, and L. Benfatto, Phys. Rev. Lett. **115**, 157002 (2015).

[51] N. Tsuji and H. Aoki, Phys. Rev. B **92**, 064508 (2015).